SEISMIC PERFORMANCE OF CONCRETE COLUMNS WITH INADEQUATE TRANSVERSE REINFORCEMENT.

Alistair Boys [1]
Des K. Bull [2]
Stefano Pampanin [3]

ABSTRACT

Existing New Zealand building stock contains a significant number of structures designed prior to 1995 with inadequate detailing of the internal or 'gravity' reinforced concrete (RC) columns. Typically these columns have insufficient transverse reinforcement, lap-splices in the plastic hinge region, and longitudinal bars that are 'cranked' at the end of the lap-splice. Columns with such details have been shown to perform poorly when subjected to seismic actions, losing shear and axial load carrying capacity at low levels of drift. A set of displacement based models are presented (and verified experimentally) for the shear failure and subsequent loss of axial capacity for these columns under both uni- and bi-directional bending.

INTRODUCTION

Existing New Zealand building stock contains a significant number of structures designed prior to the revision of NZS 3101 in 1995 with inadequate detailing of the internal or 'gravity' reinforced concrete (RC) columns. While the requirements for shear, anti-buckling and confinement lead to adequate transverse reinforcement detailing of the moment resisting frame (MRF) columns in NZS3101 1982, the 'gravity' columns did not have matching requirements. This is a considerable oversight as the 'gravity' columns undergo the same displacement demands as the MRF columns. As illustrated by previous earthquakes (see Figure 1) these columns are subject to damage associated with the displacement history of the structure, and can potentially lose axial capacity, leading to incipient collapse of the structure.

Previous studies in the United States have investigated the axial failure of similarly detailed columns. Lynn et al [1] tested eight columns (with a range of reinforcement details) uni-directionally in double curvature. These double curvature tests highlight the susceptibility of inadequately detailed columns to lose axial capacity at moderate levels of drift (~2-3%). Melek et al [2] performed six uni-directional tests on cantilever columns with lap-splices under a range of axial loads. Results from these tests are limited to information regarding cyclic deterioration of the force-displacement capacity of the columns as axial failure occurred as a result of P-δ failure as opposed to loss of axial capacity at the shear failure plane.

Both of the previous investigations focus on uni-directional bending and further research is necessary into the additional demands imposed by bi-directional bending with regard to degradation of strength/stiffness and the applicability of the proposed shear and axial drift limits.

a) Indian Hills Medical Centre (1994 Northridge Earthquake)

b) Olive View Hospital (1994 Northridge Earthquake)

Figure 1 Damage to inadequately reinforced columns during previous earthquake

1 AB, Postgraduate Student, University of Canterbury
2 DKB, Professor, University of Canterbury & Technical Director, Holmes Consulting Ltd
3 SP, Senior Lecturer, University of Canterbury

MODEL DEVELOPMENT

The most significant failure mechanism inherent in the inadequately detailed gravity columns is the loss of axial load carrying capacity. Elwood and Moehle recently proposed an idealised drift based backbone model for the drift capacity of these columns [3]. The model developed is empirical in nature and as such is applicable only to columns with appropriate reinforcement details [4]. Figure 2 below illustrates the proposed backbone capacity model and experimental results. The model has a shear capacity equal to the plastic capacity of the column (as determined by moment-curvature analysis). Detail dependent drift levels are calculated for the yielding of the section, shear failure (indicated by a reduction of capacity to below 80% of maximum); and the loss of axial load carrying capacity subsequent to the shear-failure.

For the purposes of the paper only relationships for drift at shear and axial failure will be illustrated. The drift at shear failure (δ_s) is obtained by evaluating the relationship given by Equation 1 using a shear stress (υ), corresponding to the plastic shear capacity of the section (V_p) [4].

$$\delta_s = \frac{3}{100} + 4\rho'' - \frac{1}{40}\frac{\upsilon}{\sqrt{f'_c}} - \frac{1}{40}\frac{P}{A_g f'_c} \geq \frac{1}{100} \qquad \textbf{(1)}$$

Where; ρ" = transverse steel volumetric ratio, υ = nominal shear stress, f'_c = concrete compressive strength, P = column axial load, and A_g = gross cross-sectional area.

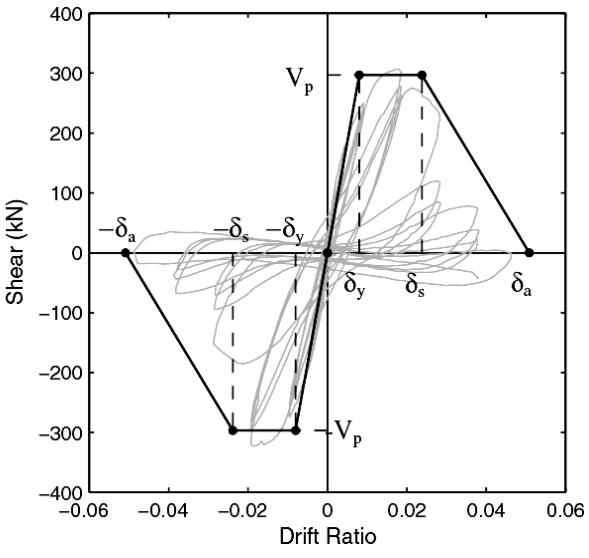

Figure 2 Backbone model with experimental data

Axial failure of the columns is dependent on prior shear failure and force equilibrium at the shear failure plane as illustrated in Figure 3. Force equilibrium in conjunction with experimental data was used to derive the relationship for the drift at axial failure [5]:

$$\delta_a = \frac{4}{100}\frac{1+\tan^2 65°}{\tan 65° + P\left(\dfrac{s}{A_{st} f_{yt} d_c \tan 65°}\right)} \qquad \textbf{(2)}$$

Where; 65° is the assumed angle of the shear failure plane, A_{st} = area of transverse reinforcement parallel to the applied shear and having spacing s, f_{yt} = yield stress of transverse reinforcement, and d_c = depth of column core measure parallel to the applied shear.

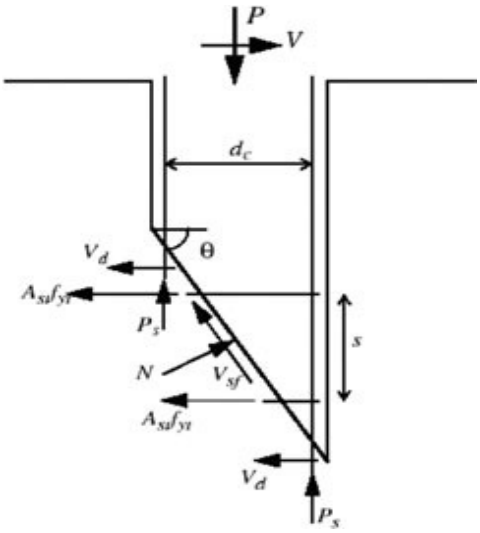

Figure 3 Free body diagram of the shear failure plane

SPECIMEN DESIGN

Design of the test columns was undertaken with consideration of the limitations imposed by the proposed models, the test apparatus, and with consultation with practising professional engineers to ensure realistic detailing. A significant detail (neglected in previous studies) is the practice in New Zealand of cranking the longitudinal bars at

the top of the lap-splice. These cranked bars are susceptible to buckling which may initiate early shear failure and loss of axial capacity.

The resulting test specimens are 450mm square cantilever columns with a height (to the application of lateral load) of 1624 mm as illustrated in Figure 4. All specimens have four D25 Grade 300 reinforcing bars (longitudinal reinforcing ratio = 1%), R10 stirrups at 300mm spacing (minimum diameter and maximum spacing allowable, transverse reinforcing ratio = 0.12%), and cranked bars at the end of the lap-splice. Two lap-splice lengths are chosen; 600mm corresponding to the minimum allowable length of 24 longitudinal bar diameters (d_b) and 750mm to reflect a more conservative design. As a consequence of the lap-splice length and the configuration of the transverse reinforcement the specimens with 24 d_b lap-splices also have inadequate restraint provided to the cranked longitudinal bars. Details of the lap-splice, cranked longitudinal bars and the location of the transverse reinforcement for the two test configurations are shown below in Figure 5.

A concrete compressive strength ($f'c$) of 32 MPa was targeted to reflect nominal design strength of 24 MPa and allowing for a 33% increase in long-term in-situ strength. Five of the specimens have an applied axial load of 2000kN reflecting the likely upper bound of existing gravity columns. The sixth test has a reduced axial load of 1000kN to enable the degradation in lateral capacity of the lap-splice to be calibrated.

The experimental program with specimen designation, detailing provided, applied axial load and imposed displacement protocol is outlined in Table 1.

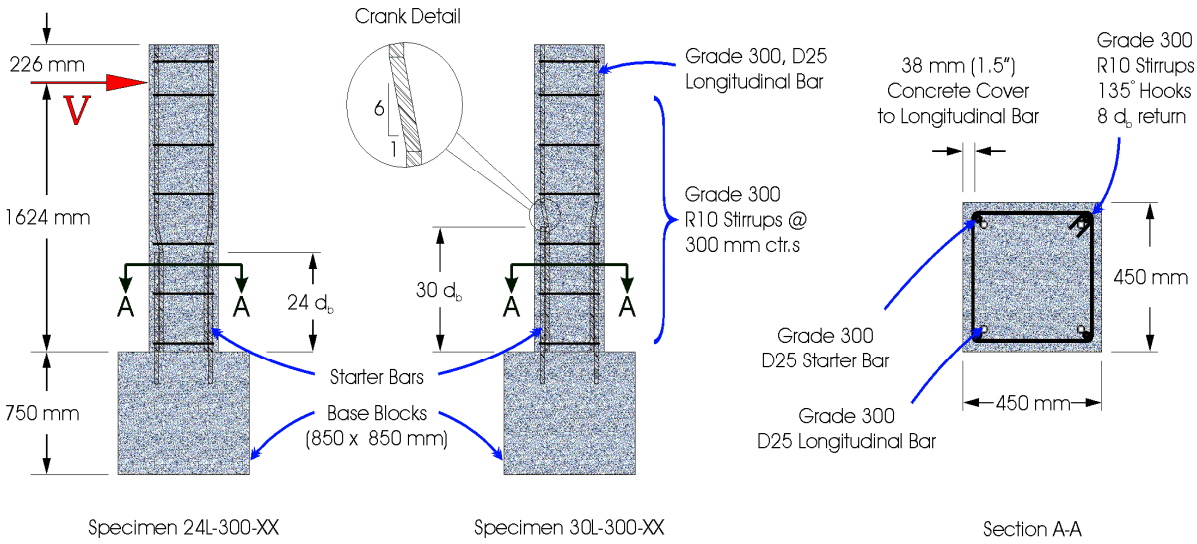

Figure 4 Details of test specimens

Table 1 Experimental program

Designation	Lap-Splice length	Tie Details	Axial Load	Loading Protocol
24L-300-2D	600mm (24 d_b)	R10 @ 300mm	2000kN (0.3f'$_c$A$_g$)	2D Quasi-Static
24L-300-3D	600mm (24 d_b)	R10 @ 300mm	2000kN (0.3f'$_c$A$_g$)	3D Quasi-Static
24L-300-3D-R	600mm (24 d_b)	R10 @ 300mm	1000kN (0.15f'$_c$A$_g$)	3D Quasi-Static
30L-300-2D	750mm (30 d_b)	R10 @ 300mm	2000kN (0.3f'$_c$A$_g$)	2D Quasi-Static
30L-300-3D	750mm (30 d_b)	R10 @ 300mm	2000kN (0.3f'$_c$A$_g$)	3D Quasi-Static
24L-300-EQ	600mm (24 d_b)	R10 @ 300mm	2000kN (0.3f'$_c$A$_g$)	3D Quasi-EQ

a) Lap-splice at base of column

b) Cranked Longitudinal bars

Figure 5 Photographs of lap-splice and cranked longitudinal bars with poorly placed stirrup

TEST APPARATUS

The test apparatus allows the cantilever columns to be loaded axially in addition to bi-axial bending. Figure 6 below illustrates the schematic of the lateral force application via a self-equilibrating frame and counterweight. Ball pivots are located at the top and base of the column allowing the reaction frame to rotate in both principal directions as the Lateral Rams extend (or contract) and induce bending in the column. Axial load is applied using the DARTECH, which has an adjustable height reaction head and a ram extending from the floor.

The experimental apparatus configured for bi-directional bending is shown below in Figure 7. The reaction frames with hydraulic rams for the two principal directions are shown. In the centre is the DARTEC, providing the axial load via a fixed reaction head upon 4 extendable legs and a 10,000kN capacity hydraulic ram at the base. Partially obscured behind the near corner leg of the DARTEC is a test specimen (following testing). In the background the counterweights can be seen.

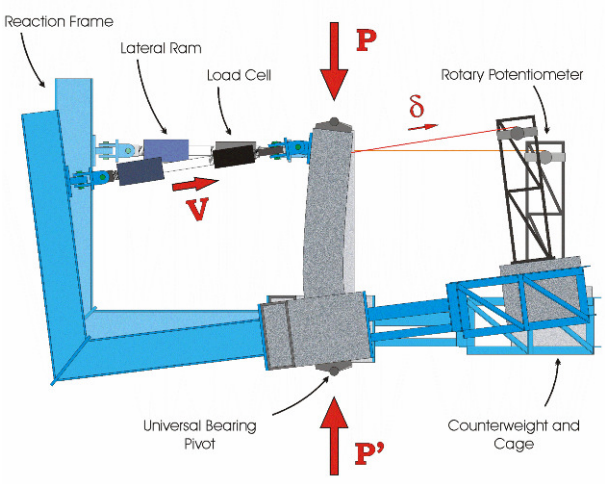

Figure 6 Schematic of experimental apparatus

Figure 7 Experimental Apparatus

MATERIAL TESTING

Prior to testing each specimen, material tests were carried out to determine; the yield strength of the longitudinal and transverse steel, and the 28 day concrete compressive strength. These results are summarised in Table 2 below. The yield strength of the longitudinal steel (f_y = 315 MPa) is very similar to the target capacity. However the yield strength of the transverse steel provided was significantly stronger (f_{yt} = 439 MPa) than was specified, however this had minimal effect on the behaviour of the specimen due to the very low transverse reinforcement ratio. There was a moderate variability in the concrete compressive strength (f'_c ranges from 24.3 to 33.6 MPa), but all values lie within the expected range of in-situ columns.

Table 2 Material testing

Column Designation	f'_c (MPa)	f_y (MPa)	f_u (MPa)	f_{yt} (MPa)
24L-300-2D	33.6	315	465	439
24L-300-3D	28.4	315	465	439
24L-300-3D-R	27.5	315	465	439
30L-300-2D	33.9	315	465	439
30L-300-3D	24.3	315	465	439
24L-300-EQ	25.3	315	465	439

UNI-DIRECTIONAL LOADING TESTS

Two specimens were tested under uni-directional loading to confirm the validity of the proposed model. Specimens 24L-300-2D and 30L-300-2D were tested using a standard quasi-static drift protocol as used by Melek et al [2]. The protocol has three excursions to positive and negative peaks at increasing levels of drift (see Figure 8).

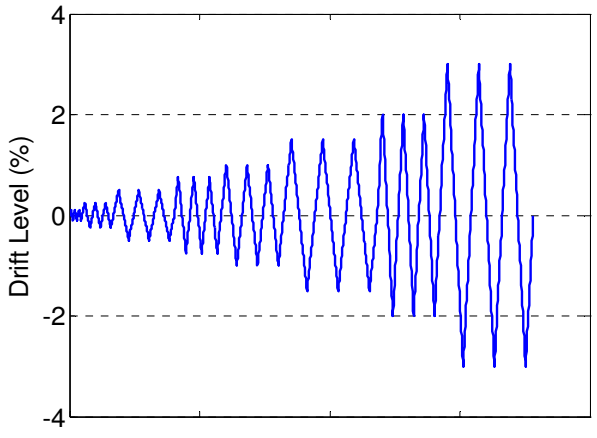

Figure 8 Uni-directional quasi-static drift protocol

The backbone model and associated drift limits for shear and subsequent axial failure were calculated for each of the specimens using the measured material strengths. Note that as the modelled axial failure is contingent on prior shear failure and the calculated drift at axial failure occurs at a lower drift than the shear failure for both specimens, the axial failure drift limit is increased to coincide with the shear failure limit.

The experimental data and model comparisons for the two tests are shown in Figure 9. Both specimens had comparable material strengths and consequently very similar backbone models. Shear failure of the two specimens occurred just prior to the modelled failure limit. Axial failure of specimen 30L-300-2D occurs simultaneously with shear failure as the model suggests and while specimen 24L-300-2D undergoes the full excursion to the peak past the drift limit, failure occurs on the subsequent reverse cycle.

Hysteretic degradation of the specimen with the minimum lap-splice length is markedly more pronounced than the more conservative specimen as Figure 9 shows. The tests also illustrate that the lack of effective restraint of the cranked longitudinal bar has no effect on the drift capacity of these columns which is perhaps counterintuitive.

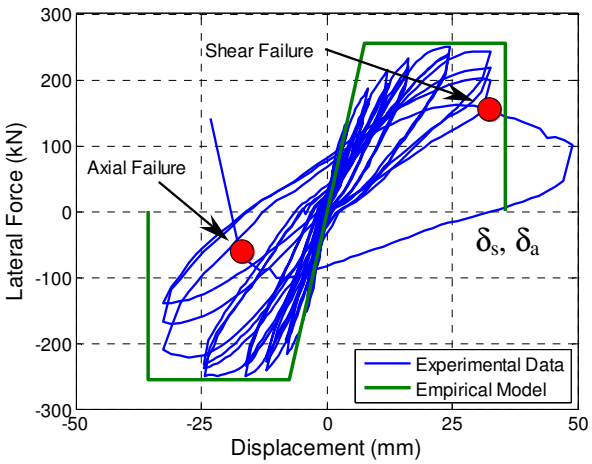

a) Specimen 24L-300-2D

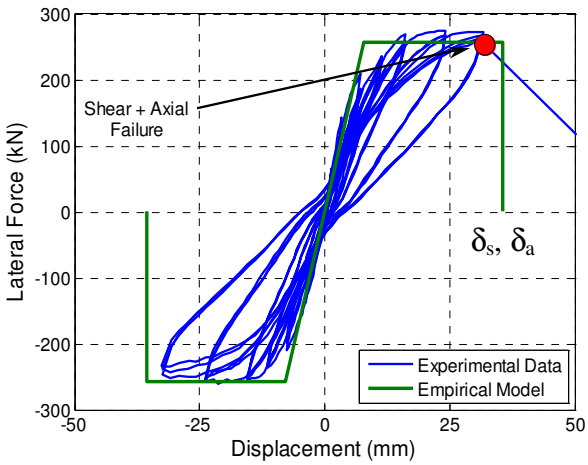

b) Specimen 30L-300-2D

Figure 9 Experimental results and empirical models for the uni-directional loading specimens

A sequence of test photographs from specimen 24L-300-2D is shown in Figure 10 a) – e) below. Comparing these with Figure 10 i) and j), the additional damage associated with the minimum splice length is apparent. Specimen 30L-300-2D exhibits minimal cracking prior to the formation of the shear failure plane and splice cover expulsion does not occur. Buckling of the longitudinal bars was isolated to the crank in specimen 24L-300-2D whereas specimen 30L-300-2D exhibited buckling in the longitudinal bar and the crank.

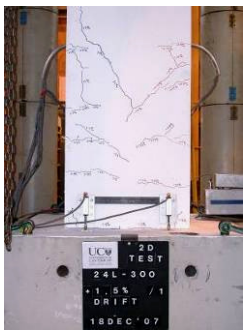

a) Specimen 24L-300-2D 1.5% Drift

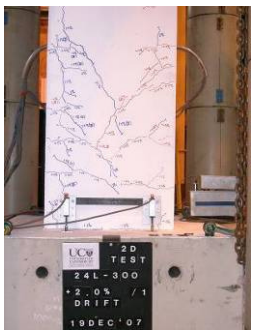

b) Specimen 24L-300-2D 2.0% Drift (1st Cycle)

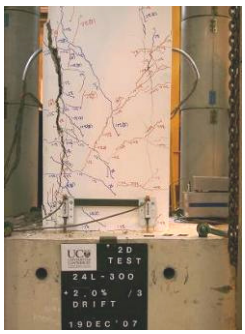

c) Specimen 24L-300-2D 2.0% Drift (3rd Cycle)

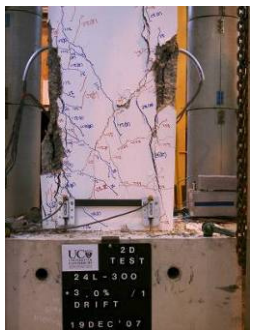

d) Specimen 24L-300-2D +3.0% Drift (shear failure)

e) Specimen 24L-300-2D -3.0% Drift (axial failure)

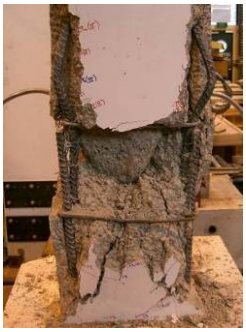

f) Specimen 24L-300-2D Buckled cranked bar

g) Specimen 24L-300-2D Burst stirrup

h) Specimen 30L-300-2D Buckled crank + Splice

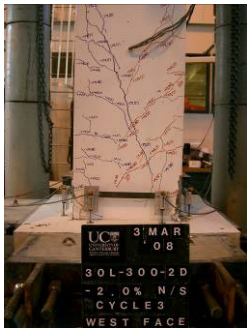

i) Specimen 30L-300-2D +2% Drift (prior to failure)

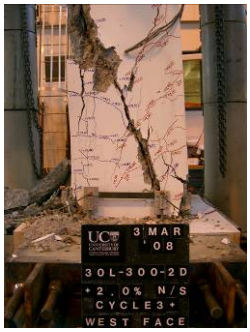

j) Specimen 30L-300-2D 2++% Drift (axial failure)

Figure 10 Progression of damage and failure close-ups

BI-DIRECTIONAL LOADING TESTS

The bi-directional loading is a modification of a 'cloverleaf' protocol. For these three tests the 'leaves' have been scaled such that the peak drift in each of the principal components is equivalent to the drift level associated with the uni-directional protocol. Each 'leaf' is traversed once at each level of drift, and in addition, an excursion is undertaken to each of the four principal axes.

Resolving the bi-directional protocol into the principal components illustrates the rationale; in each principal axes the drift protocol entails three peaks in the positive and negative directions, similar to the uni-directional protocols. As a consequence the expected increase in damage associated with bi-directional loading and the adequacy of the proposed drift based failure limits can be assessed.

Figure 11 below shows the drift protocol and experimental results for specimen 24L-300-3D (the drift protocol is identical for all three bi-directional tests). The central graph of the figure shows the drift protocol in plan view, with the components in the N-S and E-W directions shown to the right and below respectively. In addition the shear and axial failures are noted on both the Force-Displacement and the drift protocol graphs.

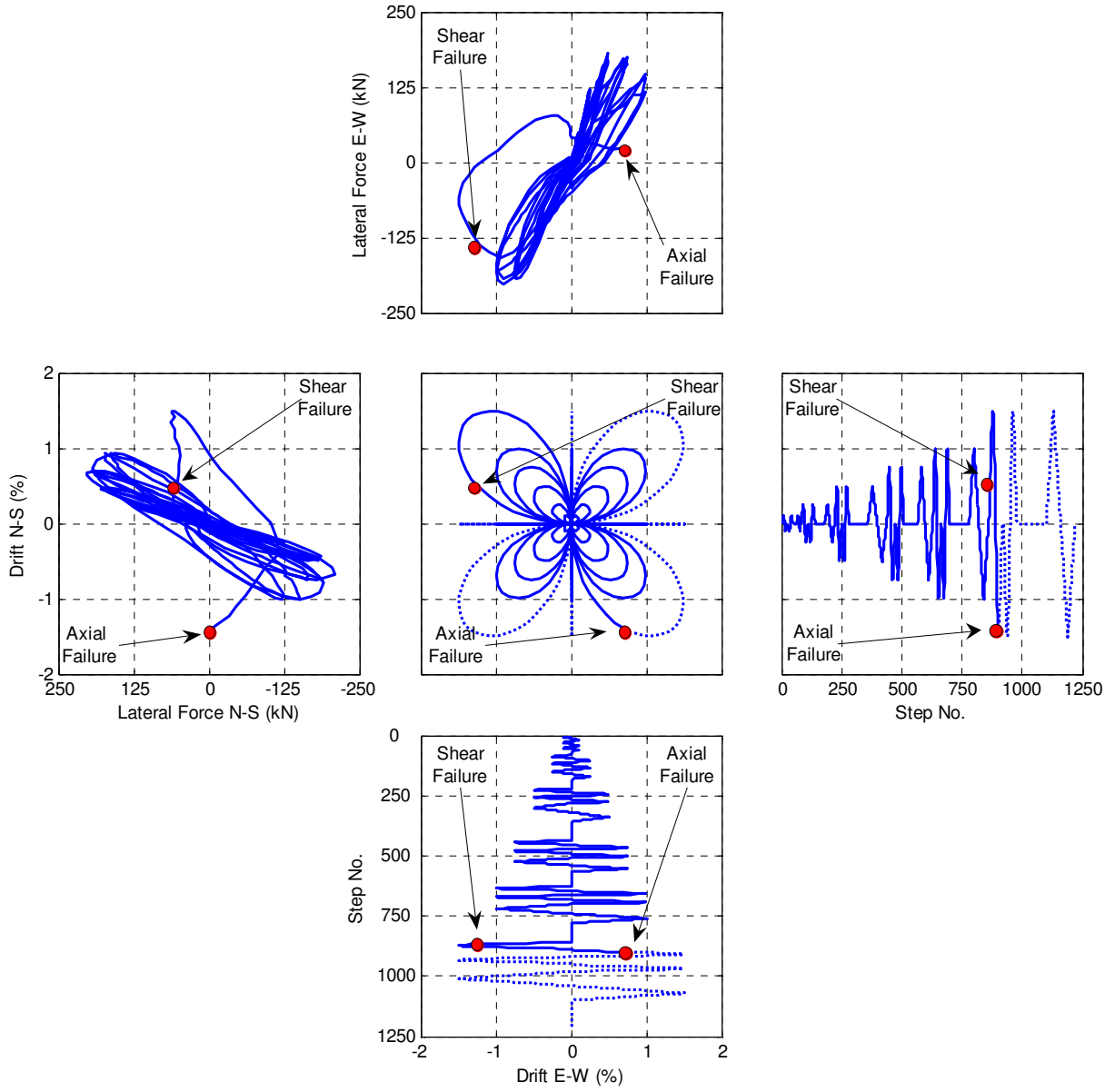

Figure 11 Specimen 24L-300-3D drift protocol and experimental results

The proposed backbone model calculates the shear and axial drift limits for unidirectional loading (for any loading angle) by assessing the section capacity (at a given loading angle) and the density and effectiveness of the transverse reinforcement. Hence for a loading angle of 45° the stirrups have a reduced effectiveness (factor of $1/\sqrt{2}$) due to geometry, affecting both the shear and axial drift limits.

Bi-directional loading poses a difficulty for this model as the section capacity and the shear and axial drift limits will differ for each angle of loading. Conservatively, it is proposed that the drift limits are calculated for loading at a 45° angle (corresponds to the minimum effectiveness of the transverse reinforcement) and resolved into the in-plane component. As the imposed loading protocol incorporates displacements through all 360°, the backbone section capacity is increased from the capacity at 45° to the capacity at 0° to include the full range of loading angles. An illustration of the backbone model for bi-directional loading (resolved to the in-plane component) is provided in Figure 12. As described previously for the uni-directional loading specimens the drift at axial failure is adjusted to coincide with the drift at shear failure.

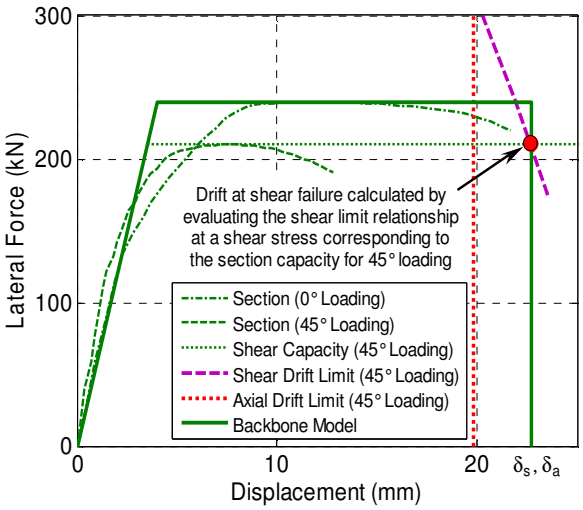

Figure 12 Backbone for bi-directional loading (resolved to the in-plane component)

Experimental results and comparison with the proposed model for the bi-directional loading tests are shown on the following page in Figure 13 to Figure 15. Looking at the relationships for specimens 24L-300-3D and 24L-300-3D-R it initially appears that the backbone model overestimates the capacity of the specimens as the force-displacement relationship does not reach the in-plane capacity. However if consideration is given to the path of the loading protocol and the high rate of degradation associated with the minimum splice length provided it is evident that full capacity is unlikely to occur. Specimen 30L-300-3D however sustains a shear force considerably closer to the backbone due to the additional capacity of the splice provided.

Of greater importance to the applicability of the model is the accuracy to predict the drift level at shear and axial failure. Experimental results and the modelled backbone for specimen 24L-300-3D are shown in Figure 13. Shear failure occurs at a level of drift slightly below the modelled level and as for the uni-directional specimen with this lap-splice length the axial failure occurs on the subsequent loop of the drift protocol.

Figure 14 shows the comparisons for the second bi-directional specimen, 24L-300-3D-R (reduced axial load of 1000kN). It is clear that the backbone model captures the shear failure and the force-displacement behaviour adequately. The notable point of departure is with regard to the drift at axial failure, which exceeds the modelled limit by approximately 50%. However if the performance of previous tests performed by Melek [2] is considered it is evident that cantilever column tests with axial load in this range lose axial capacity resulting from a flexural P-δ failure. Whereas the model developed by Elwood et al. [5] was calibrated using tests in double curvature and has shown to be valid for axial loads of this magnitude. Consequently, given the good fit of the experimental data at prior to the modelled axial failure, the performance of this model applied to real double curvature columns can be considered adequate for low axial loads.

Comparisons for specimen 30L-300-3D are shown in Figure 15. Shear failure of the specimen occurs during the first 'leaf' to 1.5% drift, just prior to the modelled limit. The subsequent axial failure occurs during the third 'leaf' of the drift protocol, slightly later than modelled limit but this could be explained by the additional restraint at the failure plane by the dowel effect of the longitudinal bars and the reduced damage associated with increased splice length.

A photographic sequence of the damage sustained by each of the three columns is shown over-page in Figure 16 - Figure 19. Similar damage is evident for each of the three tests with splice cover expulsion, bar buckling and the formation of a shear failure 'cone' being evident in all three tests. This is a result of the dependency of the modelled axial failure on the formation of a shear failure plane and the full bi-directional loading imposed on these specimens.

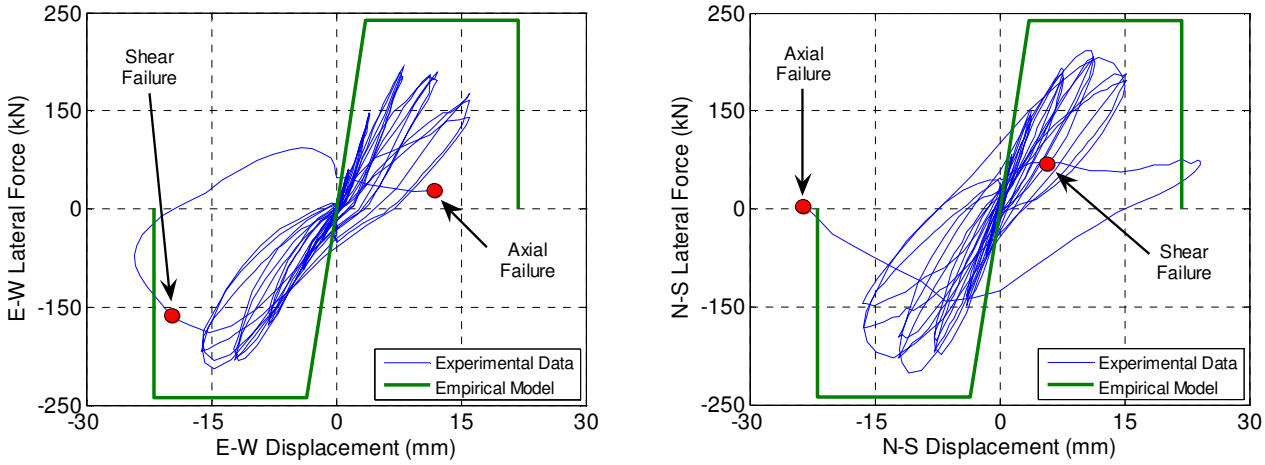

Figure 13 Experimental results and empirical models for Specimen 24L-300-3D

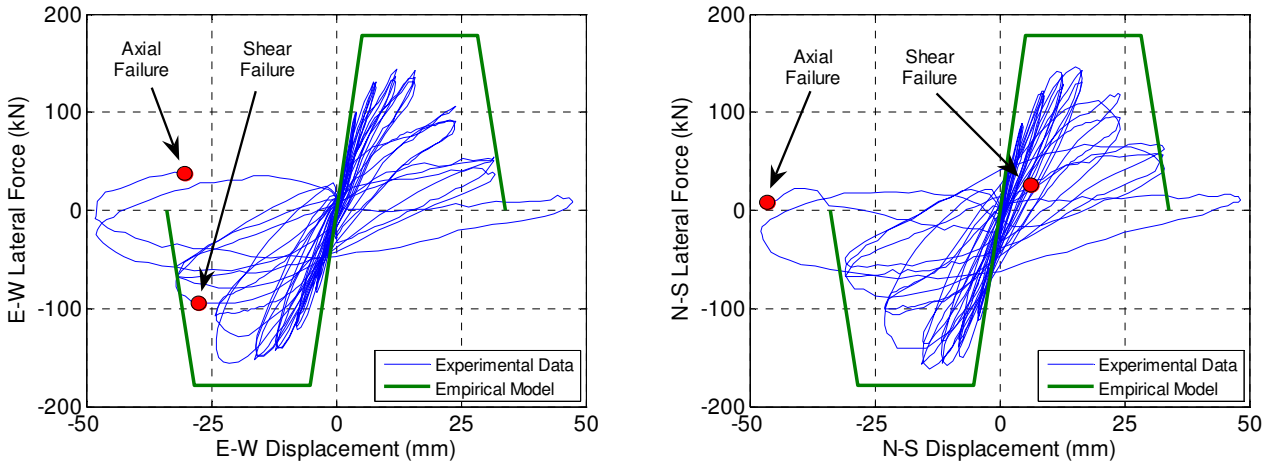

Figure 14 Experimental results and empirical models for Specimen 24L-300-3D-R

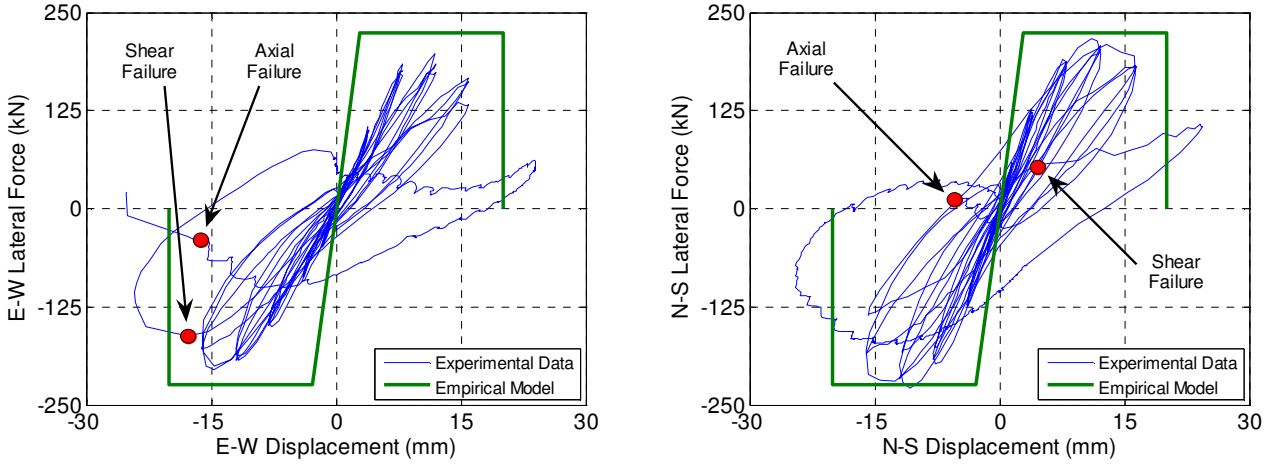

Figure 15 Experimental results and empirical models for Specimen 30L-300-3D

a) 0.5% Drift Loops **b) 0.75% Drift Loops** **c) 1.0% Drift Loops** **d) 1.5% Loop 1 (shear)** **e) 1.5% Loop 2 (axial)**

Figure 16 Progression of damage for Specimen 24L-300-3D

b) 0.75% Drift Loops **c) 1.0% Drift Loops** **d) 1.5% Drift Loops** **e) 2.0% Drift Loops** **f) 3.0% Loop 3 (axial)**

Figure 17 Progression of damage for Specimen 24L-300-3D-R

a) 0.5% Drift Loops **b) 0.75% Drift Loops** **c) 1.0% Drift Loops** **d) 1.5% Loop 2 (shear)** **e) 1.5% Loop 3 (axial)**

Figure 18 Progression of damage for Specimen 30L-300-3D

a) Specimen 24L-300-3D Buckled crank **b) Specimen 24L-300-3D Shear Failure cone** **c) Specimen 30L-300-3D Splice Cover Expulsion** **d) Specimen 30L-300-3D Cover Expulsion** **d) Specimen 30L-300-3D Buckled Bars**

Figure 19 Post failure damage photographs for bi-directional loading

QUASI-EARTHQUAKE LOADING

Development of the quasi-earthquake protocol was undertaken to determine the likely performance of these 'gravity' columns under a realistic displacement history. Also, in place of the in-plane drift limits (for 45°) used previously a full drift limit curve was derived in the NS-EW plane. The drift protocol was developed using the following steps:

1. Shear and Axial failure drift limits are calculated at 0° and 45° for the specimen (material testing required) and a limit curve is fitted.
2. A SDOF model of a prototype column is created with appropriate section properties and a hysteresis rule calibrated to the previous bi-directional tests.
3. A mass is selected to obtain an appropriate period to ensure relevant excitation from the earthquake record.
4. Earthquake record selection was made using the GNS database records for Wellington, given a standard shallow earthquake, and ensuring that the demand was not too excessive in terms of a large number of peaks near the limit curve. To this end the two orthogonal components of the F78201Z2 record of the 1978 Tabas earthquake were selected.
5. The record components are scaled to obtain a displacement history that coincides with the calculated drift limits for axial failure.

Figure 20 below illustrates the imposed displacement protocol for specimen 24L-300-EQ and the experimental results with the modelled in-plane backbone limits. The central graph of the figure shows the protocol and limit curve, with the components in the N-S and E-W directions shown to the right and below respectively.

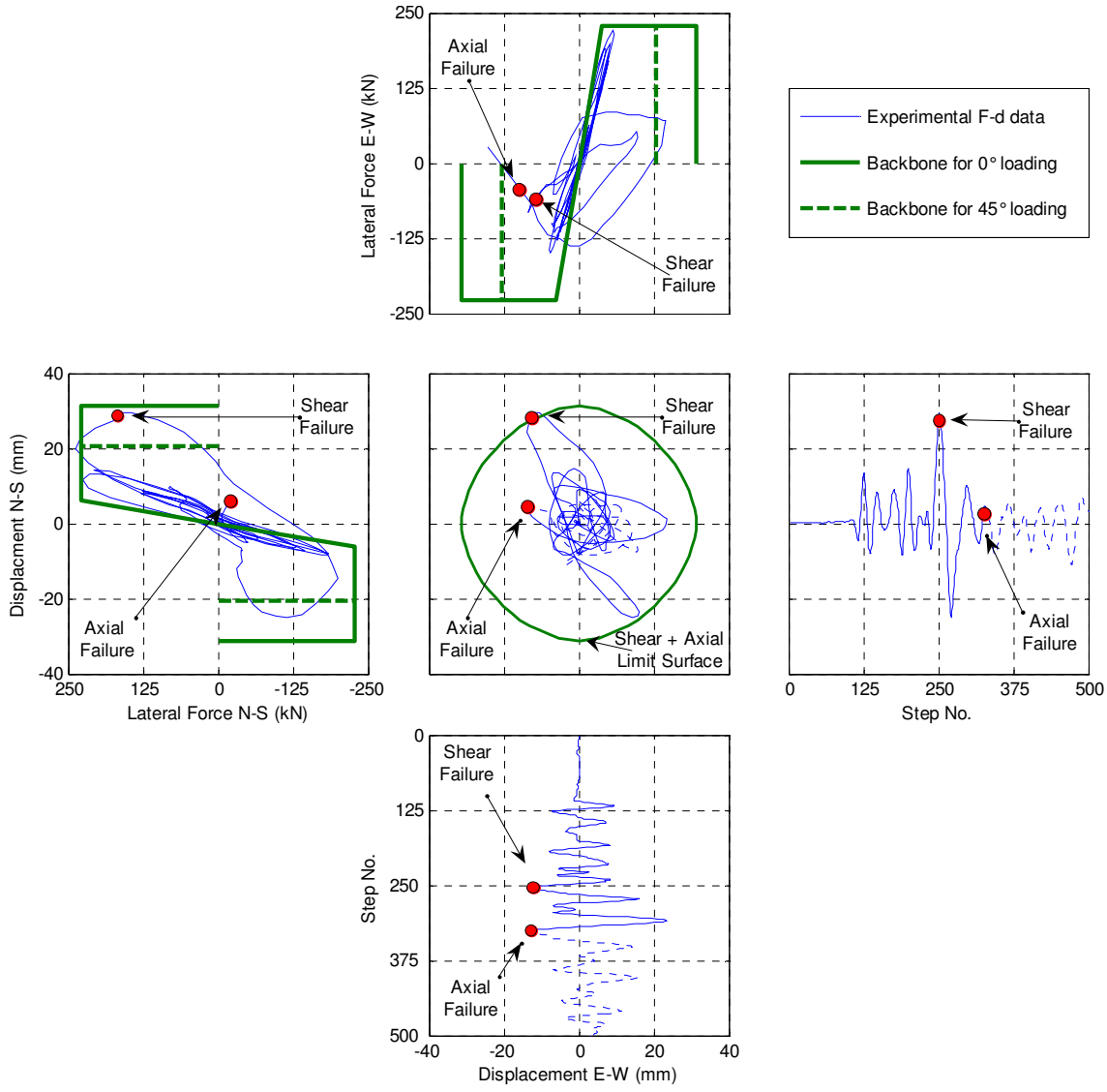

Figure 20 Specimen 24L-300-EQ experimental results and model comparison

The comparison between the experimental data and the backbone model with drift limit curve(s) (shear and axial drift limit curves coincide for this specimen) illustrates the necessity to assess the full bi-directional behaviour of these columns. Shear failure occurs as the bi-directional drift reaches the limit curve, however if the in-plane representation of the backbone is considered failure occurs between the solid and dashed backbone lines correspond to drift capacity for in-plane and 45° loading respectively. As is evident the angle at which the drift maxima occurs affects the drift capacity, thus assessing columns using the 45° limits is conservative and the full limit curve should be used.

Several excursions to significant levels of drift beyond the shear failure are required for axial failure to occur. However as earthquake records generally follow this post-peak pattern (with the exception of near-field events) it is appropriate to accept the validity of the drift-based backbone model and associated limit curves.

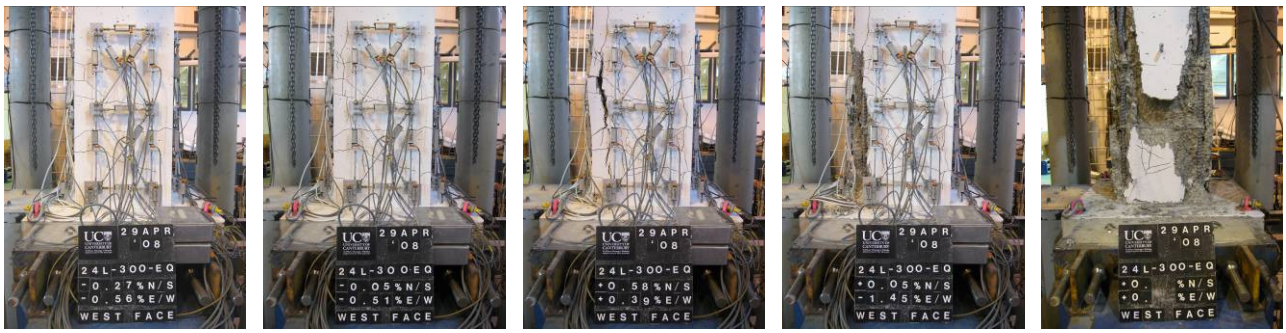

b) Specimen 24L-300-2D 1.5% Drift | **c) Specimen 24L-300-2D 2.0% Drift (1st Cycle)** | **d) Specimen 24L-300-2D 2.0% Drift (3rd Cycle)** | **e) Specimen 24L-300-2D +3.0% Drift (shear failure)** | **f) Specimen 24L-300-2D -3.0% Drift (axial failure)**

Figure 21 Progression of damage for Specimen 24L-300-EQ

CONCLUSIONS

This investigation into the performance of RC gravity columns under uni- and bi-directional loading leads to the following conclusions:

1. RC gravity columns with inadequate transverse reinforcement are extremely susceptible to loss of axial load carrying capacity at drift levels lower than allowable during a design level event.
2. The backbone model proposed by Elwood and Moehle [3] is confirmed to adequately capture the shear and axial failure drift limits of RC columns with inadequate transverse reinforcement, including the extension to bi-directional loading.
3. Bi-directional loading results in a significant reduction to the in-plane drift capacity, however if a pair of shear and axial failure limit curves are used when assessing these columns the drift capacity may be more accurately assessed.
4. Buckling of the poorly restrained cranked longitudinal bars is not a critical mechanism for loss of axial load capacity.
5. The lap-splice length provided does not affect the drift capacity of RC columns, but does affect the rate of degradation and damage.

REFERENCES

[1] A. C. Lynn, J. P. Moehle, S. A. Mahin, and W. T. Holmes, "Seismic Evaluation of Existing Reinforced Concrete Building Columns," *Earthquake Spectra*, vol. 12, pp. 715-739, 1996.

[2] M. Melek, J. W. Wallace, and J. P. Conte, "Experimental Assessment of Columns with Short Lap Splices Subjected to Cyclic Loads," *PEER Report*, vol. 04, 2003.

[3] K. J. Elwood and J. P. Moehle, "Idealised Backbone Model For Existing Reinforced Concrete Columns and Comparisons With FEMA 356 Criteria," *Struct. Design Tall Spec. Build.*, vol. 15, pp. 553-569, 2006.

[4] K. J. Elwood and J. P. Moehle, "Drift Capacity of Reinforced Concrete Columns with Light Transverse Reinforcement," *Earthquake Spectra*, vol. 21, pp. 71-89, 2005.

[5] K. J. Elwood and J. P. Moehle, "Axial Capacity Model for Shear-Damaged Columns," *ACI Structural Journal*, vol. 102, pp. 578-587, 2005.